coatings

MDPI

Article

The Mode Deformation Effect on Surface Nanocrystalline Structure Formation and Wear Resistance of Steel 41Cr4

Volodymyr Kyryliv [1], Olha Maksymiv [1], Volodymyr Gurey [2], Ihor Hurey [2,3], Yaroslav Kyryliv [4,*] and Olha Zvirko [1]

[1] Department of Diagnostics of Materials Corrosion-Hydrogen Degradation, Karpenko Physico-Mechanical Institute of the NAS of Ukraine, 5, Naukova St., 79060 Lviv, Ukraine
[2] Department of Robotics and Integrated Mechanical Engineering Technologies, Lviv Polytechnic National University, 12, Bandera St., 79013 Lviv, Ukraine
[3] Faculty of Mechanics and Technology, Rzeszow University of Technology, 12, Powstancow Warszawy St., 35-959 Rzeszow, Poland
[4] Department of Organization of Scientific and Research Activities, Lviv State University of Life Safety, 35, Kleparivska St., 79007 Lviv, Ukraine
* Correspondence: yaroslav_kyryliv@ukr.net; Tel.: +380-(32)-233-2479

Abstract: A surface nanocrystalline steel layer in the low alloy steel 41Cr4 was fabricated by using mechanical-pulse treatment (MPT) with different deformation modes. The structure parameters, the physical and mechanical properties, the wear resistance, and the surface topography parameters of the treated steel depending on the deformation mode were investigated. A tool with a smooth working surface was used for inducing unidirectional deformation in the top surface layer (shear), and a tool with the oppositely directed grooves was used for generating multidirectional deformation. The surface layer with a nanocrystalline structure formed by MPT using both of the tools was characterised by enhanced mechanical properties and wear resistance compared with those of the untreated or heat-treated steels. Inducing multidirectional deformation during the MPT resulted in a decrease in the grain size and an increase in the depth and microhardness of the surface layer due to it facilitating the generation of dislocations compared to those formed under unidirectional deformation. The results also demonstrated that favourable surface topography parameters providing the highest wear resistance of the steel were obtained at MPT using multidirectional deformation.

Keywords: nanocrystalline structure; white layer; surface topography; Abbott–Firestone diagram; wear resistance; grain size

Citation: Kyryliv, V.; Maksymiv, O.; Gurey, V.; Hurey, I.; Kyryliv, Y.; Zvirko, O. The Mode Deformation Effect on Surface Nanocrystalline Structure Formation and Wear Resistance of Steel 41Cr4. *Coatings* **2023**, *13*, 249. https://doi.org/10.3390/coatings13020249

Academic Editor: Yanxin Qiao

Received: 17 December 2022
Revised: 11 January 2023
Accepted: 18 January 2023
Published: 21 January 2023

1. Introduction

Extreme operating conditions, namely the simultaneous action of mechanical loading and wear, demand the highest performance of the materials used in many industries [1–3]. It is well known that the wear resistance of materials is highly susceptible to the microstructure and properties of the material surface [4]. Many techniques are used to obtain surfaces with a high resistance to wear, such as mechanical processing, chemical processing, laser processing, plasma processing, gas nitriding, ion implantation, and many others [1,3–6]. Recently, materials with a nanocrystalline structure (NCS) in the top surface layer have been considered as promising candidates for operation in such severe conditions [7–11]. The generation of a surface NCS enables the protection of the metal surface and significantly enhances the overall properties.

One of the most widely used methods for the formation of an NCS is the severe plastic deformation (SPD) methods [10–12]. They have become widespread in the production of nanocrystalline metals and alloys due to their capability to refine the grain size of the materials at the nanometer scale of large-scale components, which results in improved mechanical properties. Among of these techniques, a mechanical-pulse treatment (MPT) is

an effective way to generate nanocrystalline surface layers by high-speed friction [11,13]. The high-density dislocations near the surface resulting from SPD during the MPT is accompanied by the simultaneous quenching and alloying of the surface metal layer; these processes have finally resulted in the generation of an NCS. The advantage of the MPT over the other SPD methods (hard turning, vibrational balls hardening, an ultrasonic impact treatment, etc.) [14–25] consists of the formation of surface NCSs with high depth (up to 300 μm) and high microhardness values [11]. Moreover, alloying during the MPT plays an essential role in the stabilization of the NCS. It was demonstrated in [26] that carbon segregated on the subgrain boundaries in a ferrite stabilised structure had a subgrain size of lower than 10 nm.

The degree of SPD is limited by the nucleation of dislocations and their movement. The generation of dislocations in metals and alloys is generally associated with the Frank–Read source. Multiple cross-sliding is a simple and effective mechanism of achieving dislocation multiplication, which reduces the creation of a dislocation line with a great length moving from one parallel plane to another [27]. However, nanocrystalline materials usually show a behaviour which differs from the conventional coarse-grained materials [27], and the possibility of realizing the Frank–Read mechanism in nanomaterials is still under discussion [28–30]. Nevertheless, the nucleation and propagation of dislocation are very important factors for the generation of NCS. Therefore, the mode of deformation could influence grain refinement during SPD. Usually, the SPD is imposed on the surface layers by unidirectional shear strain (hot rolling and sliding, etc.). To induce multidirectional deformation during the generation of the surface NCSs using MPT, a special strengthening tool with oppositely directed grooves (on the tool's periphery) was developed [31]. It was demonstrated [31] that it enables the formation of a nanostructure with a lower energy expenditure and higher dislocation density and, therefore, with a lower grain size in the top surface layer and a greater thickness compared with that which is generated using unidirectional deformation. The application of a multidirectional SPD resulted in increasing wear resistance, contact, and corrosion fatigue, and the decreasing hydrogen permeability of the nanostructured materials [11,32–36].

The purpose of the study was to form surface nanocrystalline layers on low alloy steel 41Cr4 by the SPD method with different modes using the MPT and to evaluate their structure, their physical and mechanical properties, wear resistance, and their surface topography.

2. Materials and Methods

The low alloy steel 41Cr4 was investigated. The chemical composition of the steel is as follows, mass. %: 0.40 C; 0.78 Mn; 0.26 Si; 1.12 Cr; 0.01 S; 0.01 P; Fe: balance. The steel in the as-delivered state had a ferrite-pearlite microstructure.

Two series of samples with different geometry were used for the formation of the surface NCS by MPT: cylindrical samples with a diameter of 40 mm and a length of 200 mm and flat samples measuring 20 × 40 × 100 mm.

From the cylindrical samples, after the MPT, we cut out specimens in the form of rings for the wear investigations; these were the specimens for metallographic analysis and microhardness measurements. Ring specimens with the same dimensions as those in the wear tests were manufactured and subjected to a heat treatment (quench-hardening and low-temperature tempering at 150 °C) in order to compare the wear resistance of the studied steel in the different states (heat-treated one and that with the surface NCS). The flat specimens were used for the X-ray analysis, electron microscopy study, and surface topography investigation. Additionally, the flat specimens with the dimensions of 10 × 20 × 100 mm were subjected to a heat treatment (quench-hardening and low-temperature tempering) with the purpose of performing a comparison of the surface topography parameters.

2.1. The Technology of MPT

This is based on high-speed friction. According to kinematics, the MPT is similar to grinding. For its implementation, we used modernised surface or circular grinding machines (Jotes, Krakow, Poland) (which were used for strengthening the flat or cylindrical surfaces, respectively) and lathes with a device with an autonomous tool drive, which was installed instead of the tool post (Figure 1). A metal tool is installed instead of a grinding wheel. A linear speed of 60–80 m/s is required for the formation of a highly concentrated energy source in the contact zone of the tool with the processed surface, as determined using mathematical modelling and a simulation and confirmed experimentally [37]. For this purpose, the modernization of the main drive of the machine spindle was carried out. During the MPT process, the working surface of the tool is pressed to the strengthening surface of the treated part. Consequently, a load of approx. 0.8−1.0 GPa is induced in the contact zone, which was estimated by analysing the relationship between the applied load and the area of the friction contact zone during the MPT [31]. Additionally, a technological medium is applied to the processing area during the MPT.

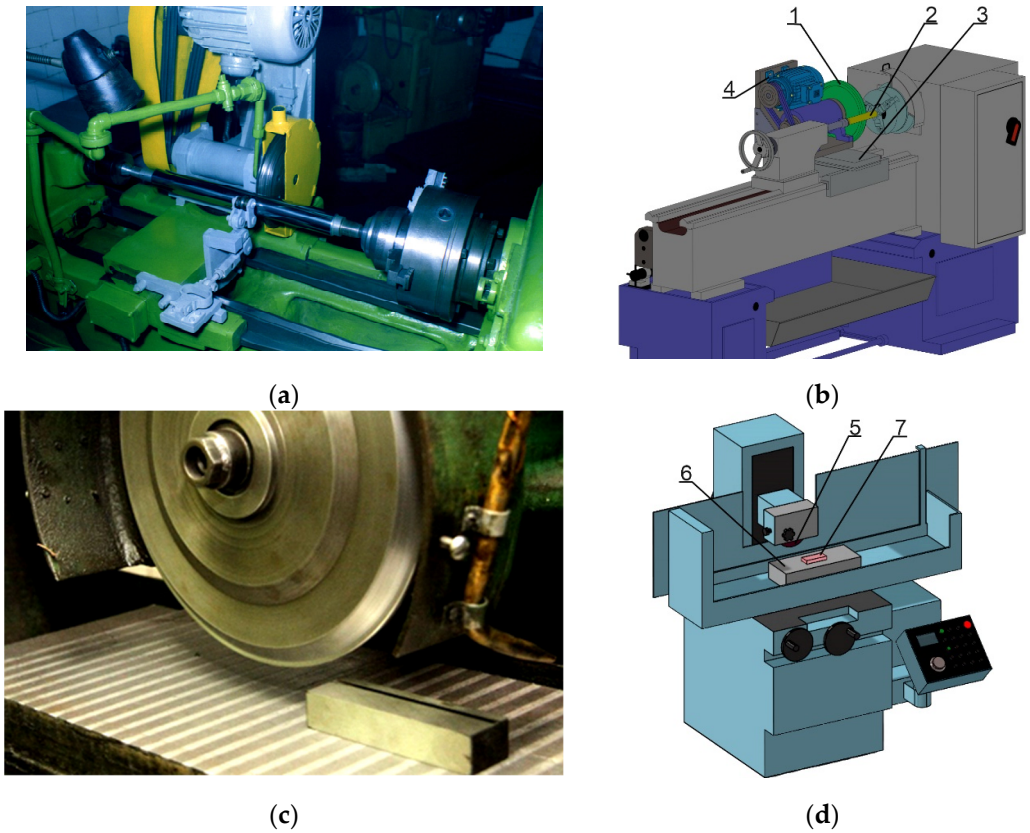

Figure 1. Lather (**a**) and the setup for the MPT of the cylindrical surface of machine parts (**b**): 1—tool; 2—specimen with the cylindrical surface; 3—carriage; 4—the device with an autonomous tool drive. Surface grinding machine (**c**) and the setup for the MPT of the flat surface of machine parts (**d**): 5—tool; 6—table of the machine; 7—specimen.

During the MPT, the treated specimen is subjected to severe thermoplastic deformation with simultaneous heating treatments up to a temperature of 700–1100 °C due to high-speed friction, and after that, it is rapidly cooled due to the heat transferring into the treated specimen, the tool, and the technological medium. High temperatures activate the dislocation movement. The deformation rate is ~10^3 s^{-1}; it characterises the rate of the accumulation of defects and, accordingly, the rate of structure dispersion. The MPT of steels resulted in the formation of the surface layer with a gradient NCS with a grain size of

12–60 nm at the top, structural-phase transformations, and saturation by the components of the technological media due to their destruction during the MPT [11,13].

Two different strengthening tools were used for the MPT (Figure 2): one with the smooth working surface (Figure 2a) and one with the oppositely directed grooves placed at an angle of 45° to a vector of rotation of the tool (Figure 2b). The tool diameter was 250 mm, and the width of the working surface was 6 mm. The width of the groove on the work surface of the tool was 4 mm (Figure 2b). The working parts of the tools were made of medium carbon steel C45. The tool with the oppositely directed grooves on the working part provides the optimal system of fragmentation of the structure in three mutually orthogonal planes of sliding compression and shear in two directions (the velocity vector of the tool and the axis of its rotation, respectively). This means that there is an additional direction of deformation of the treated surface layer, which is perpendicular to the velocity vector of the tool, compared to the tool with the smooth working surface. The parallel movement of the sliding planes in the axial direction of the tool improves the dislocation generation and structure dispersion at the nanoscale and decreases the expenditure of energy for MPT.

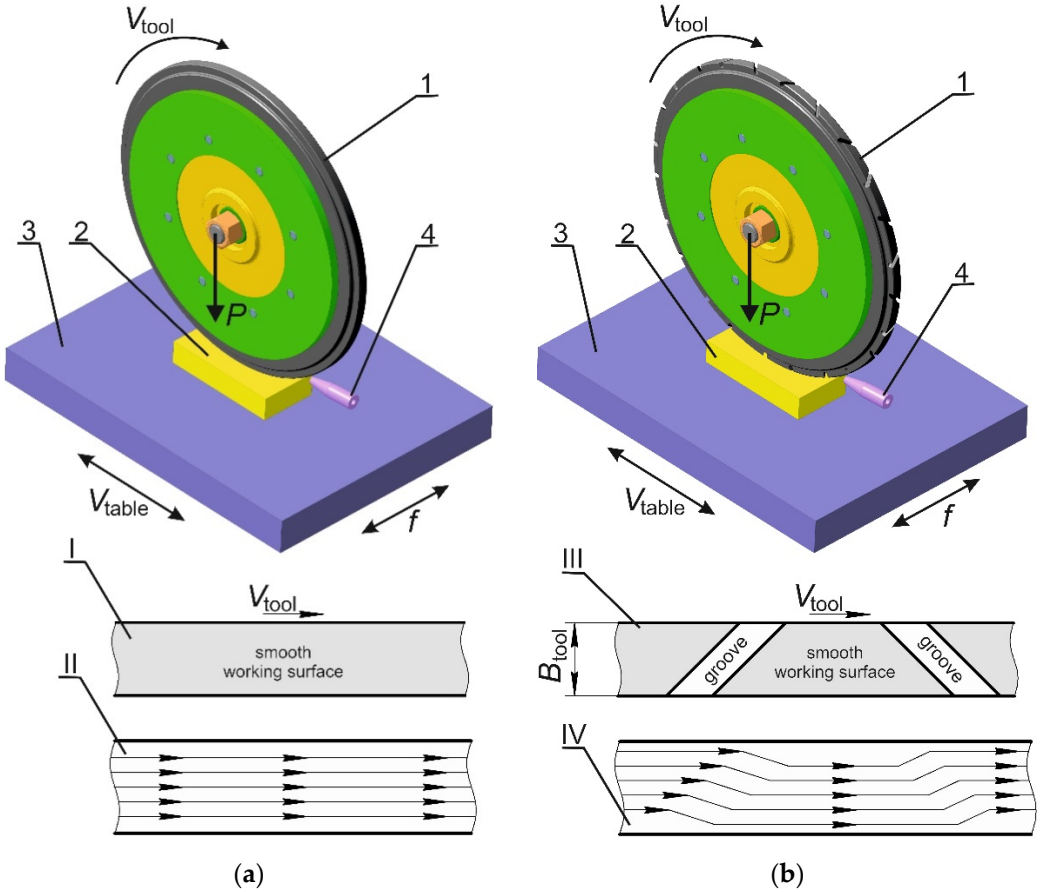

Figure 2. Scheme of MPT of flat specimens by using the strengthening tools with the smooth working surface (**a**) and with the oppositely directed grooves on the working surface (**b**): 1—tool; 2—specimen; 3—table of surface grinding machine; 4—nozzle for delivery of technological medium; working cross-sections (I, III) and directions of shear deformation (II, IV) of strengthening tools with the smooth working surface (I, II) and with the oppositely directed grooves on the working surface (III, IV). V_{tool} is *linear speed of the strengthening tool*, V_{table} is *speed of the machine tool's table* and f is *a transverse feed of the strengthening tool*.

The MPT of the specimens' cylindrical surfaces was carried out using a modernised lathe. The piece of equipment with an autonomous drive of the strengthening tool was

installed instead of the tool post, which provided a linear velocity of 60 m/s on the periphery of the tool. The surfaces of the flat specimens were subjected to the MPT using a modernised surface grinding machine. Instead of a grinding wheel, a metal tool disc was installed on the machine.

Mineral oil with the additive of low-molecular polyethylene for additional carburizing [11] during the MPT was used as a technological medium.

2.2. Test Methods

The phase composition and average grain size L of the steel's surface layer after the MPT were determined by X-ray analysis using the diffractometer DRON-3 (Research and Production Association "Burevestnik", Leningrad, USSR) of with a CuK_α X-ray source (a voltage of 30 kV, and an intensity of 20 mA), a spacing of 0.05°, and the exposition of 4 s. The diffractograms were post-processed using the software CSD (version 8.6) [38]. The X-ray diffraction patterns were analysed using the Joint Committee on Powder Diffraction Standards/American Society for Testing and Materials (JCPDS-ASTM) index [39].

The structure was investigated using an optical microscope Neophot-21 (Carl-Zeiss, Jena, Germany), and the microstructure was investigated using an EVO 40 XP scanning electron microscope (Carl-Zeiss, Jena, Germany).

The microhardness H_μ was measured using the microhardness testing machine PMT-3 (LOMO, Leningrad, USSR) at a load of 50 g on the metallographic sections made from the flat specimens of steel 41Cr4. The Vickers hardness tests were carried out using a standard 136-degree pyramidal diamond indenter.

Microhardness was determined by Formula (1):

$$H_\mu = 1854 \cdot P/d^2, \quad (1)$$

where P is the load; d is the diagonal of the square indent.

The wear behaviour of the specimens was evaluated by a sliding wear test using the friction and wear testing machine (Test Instrument Factory, Ivanovo, USSR) according to the insert-on-ring scheme (Figure 3). The wear tests were performed at a sliding speed of 1 m/s with normal loads of 1 MPa. Before the beginning of the tests, the friction pairs were run in to stabilise the friction moment and to fit the connecting surfaces, which was estimated by the presence of friction marks on an area of at least 90% of the working friction surface of each specimen. The duration of the friction pair tests was 6 h, which corresponds to the running distance of 17×10^3 m. Wear resistance was estimated by the weight loss. Before weighing them, the rings and inserts were washed using alcohol and dried. The weight loss of the specimens was determined by weighing them before and after the wear tests using an analytical weight with an accuracy of 0.2 mg.

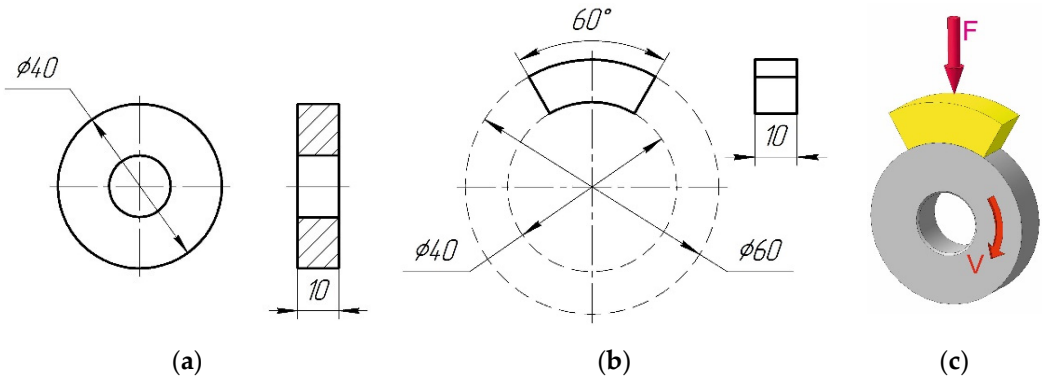

Figure 3. Drawings of ring specimens (**a**), insert specimens, (**b**) and schematic diagram of the friction pair (**c**). Φ is diameter designation, F is normal load and V is sliding speed.

The investigated ring specimens (diameter—40 mm; width—10 mm) were made of steel 41Cr4. The insert specimens were made of grey cast iron GJL-200 in the form of a segment, with a width of 10 mm, and the contact area was 200 mm^2. In the tribological systems without lubrication, quench-hardened steel is often coupled with cast iron due to its antifriction properties. The fixed insert specimen was connected to the differential sensor of the dynamometer, and it recorded the friction between the pair. The coefficient of friction was determined as the ratio between the friction force and the normal force. Thermocouples with a diameter of 0.2 mm were mounted to the insert specimen. The signals from the thermocouple recorded the temperature above the friction area at a depth of 0.2–0.3 mm.

The working surfaces of the rings were strengthened using the MPT; the working surfaces of the inserts were non-strengthened, and they were only ground to a surface roughness of 0.6 μm. The non-strengthened friction pairs were used for comparison; the working surfaces of the rings were ground after quench hardening and low-temperature tempering to a surface roughness of 0.6 μm. The wear resistance of the rings after the MPT was compared with that after the heat treatment. The ring specimens after the MPT were not subjected to any additional treatments.

The surface topography and roughness of the specimens after the MPT were studied using a three-dimensional profilometer Talyscan 150 (Taylor Hobson Precision, Leicester, UK). The analysis of the obtained results was carried out using the software Digital Surf Mountains Lab Premium (version 8.2) according to ISO 25178-26:2012 [40].

3. Results and Discussion

Metallographic studies have shown that the nanostructured surface layer in the form of a white non-etching zone (so-called white layer) is generated during the MPT of the steel 41Cr4 using both of the tools (Figure 4). The thickness of the strengthened layer is ~160 μm after the treatment using the tool with the smooth working surface, and it increases up to approx. 240 μm after the treatment using the tool with the oppositely directed grooves (Figure 4a,b).

The microhardness of the strengthened layers obtained during the MPT using tools with different shapes of the working surface is a little different, and it is 8.58–9.13 GPa (Figure 5). However, it is significantly higher than that of the base metal structure, which is equal to 1.7 Gpa. The increasing microhardness of the surface top layer of steel 41Cr4 after the MPT using the tool with the oppositely directed grooves (Figure 5, curve 2) is a result of the generation of multidirectional deformation during the treatment, facilitating the nucleation of dislocations and, consequently, structure fragmentation. Simplifying the dislocations' generation provides an increment in the depth of the treated layer with the NCS. The formation of the NCS is significantly accelerated during the MPT, since pressure, temperature, and speed of the deformation are greatly higher compared with those of other methods of surface nanostructurization (hard turning, shot peening, and ultrasonic treatments, etc.) [10,11,15,19].

The XRD of the surfaces of steel 41Cr4 after the MPT using the different tools has been examined (Figure 6) to analyze the phase composition. The martensite structure and the martensite-austenite structure were determined by a X-ray structural analysis of the surface layer after the MPT using the tool with the smooth working surface and that with the oppositely directed grooves on the working surface, respectively. Traces of the γ-phase were detected in the XRD pattern of the specimen after the MPT using the tool with the smooth working surface. However, its content increased to a mass of 3.2% after the MPT when we were using the tool with the oppositely directed grooves on the working surface.

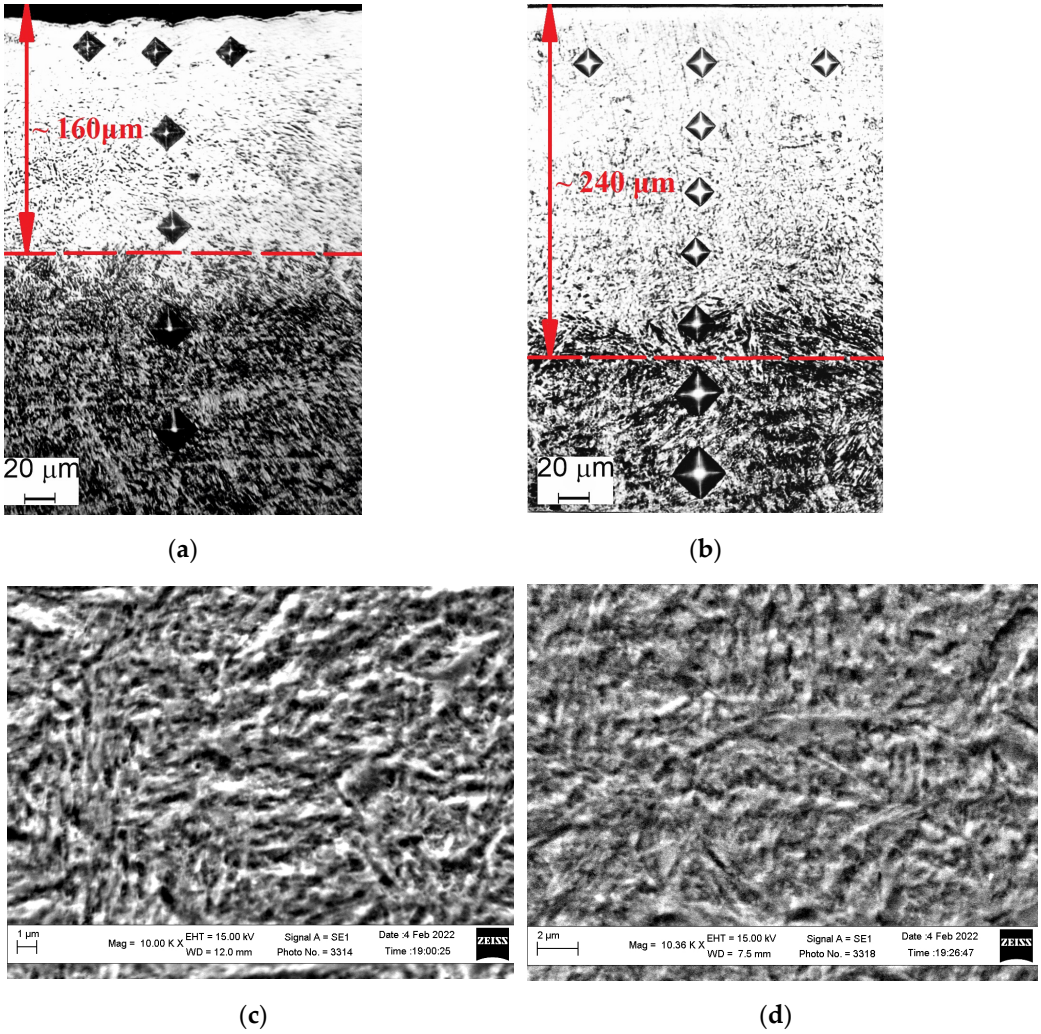

Figure 4. Structure and electron microscope images of the steel 41Cr4 after the MPT by using different tools: with the smooth working surface (**a**,**c**); with the oppositely directed grooves on the working surface (**b**,**d**). Deciphering the designations for (**a**,**b**): (◈)—*microhardness indantation imprints*; (◄►)—*an arrow that shows the depth of the hardened layer*.

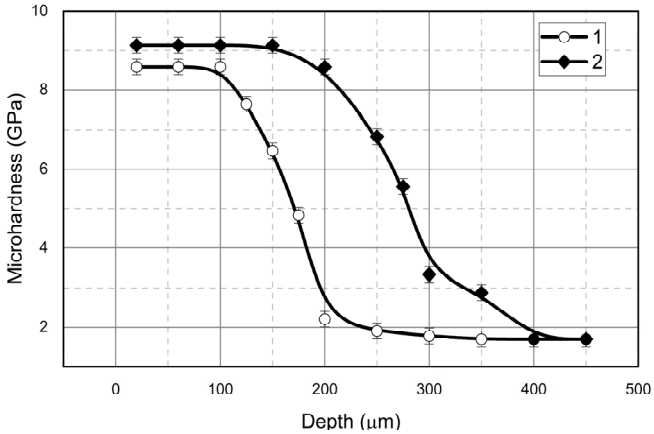

Figure 5. Microhardness of the surface layer of the steel 41Cr4 (EN) after the MPT using different tools: 1 (○) —with the smooth working surface; 2 (♦)—with the oppositely directed grooves on the working surface.

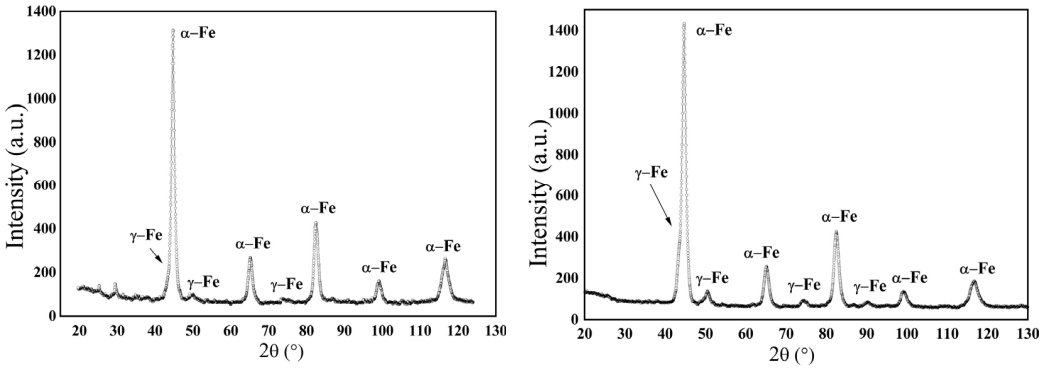

Figure 6. The XRD of the specimens of steel 41Cr4 after the MPT using the tool with the smooth working surface (**a**) and with the oppositely directed grooves on the working surface (**b**).

Data of X-ray analysis of the α-phase of the surface NCS layer of the studied steel after the MPT using the different tools are presented in Table 1. The high imperfection of the obtained nanostructure using the tool with the oppositely directed grooves on the working surface (Table 1) decreases the stacking fault energy and suppresses the return process. The structure of the surface layers is highly fragmented, especially after processing using the tool with the oppositely directed grooves on the working surface.

Table 1. X-ray parameters [1] of the α-phase of the surface NCS layer of steel 41Cr4 after the MPT using the different tools.

MPT	$B_{(110)}$	$B_{(310)}$	L, nm	ε, %	$\varrho \cdot 10^{13}$, cm^{-2}	a, nm
Tool with the smooth working surface	0.682	1.552	10.7 ± 0.8	0.077	0.48	0.28654
Tool with the oppositely directed grooves	0.873	1.807	8.6 ± 0.6	0.086	0.65	0.28642

[1] In Table 1, B(110) and B(310) are the physical broadening of maximums (110) and (310) of α-phase, respectively; L—the average size of the coherent-scattering region, nm; ε—the lattice relative deformation, %; = ϱ—the dislocation density, cm^{-2}; a—the parameter of the unit cell (lattice), nm.

The cumulative value of the grain size L of α-phase determined by X-ray analysis at the penetration of the X-ray beam at ~18 μm from the surface was 10.7 nm after the MPT using the first tool and 8.6 nm after the MPT using the second one (see Table 1). The difference in the average grain sizes observed for the steel treated using different tools can be explained by the higher degree of plastic deformation during the MPT using the tool with the oppositely directed grooves, which was confirmed by a higher dislocation density = ϱ (0.65 cm^{-2}) and lattice relative deformation ε (0.086%) (see Table 1).

The formation of a nanostructure in the strengthened layer using the MPT was confirmed by the TEM images of steel C45 in this paper [13] (Figure 7). The results are presented as dark field images (Figure 7a,c) and diffraction patterns (Figure 7b,d) at the depths of 5 μm and 10 μm. The parallel colonies of grains with a size of less than 10 nm (Figure 7a) and a curved grain boundary (Figure 7c) were revealed. The grains were significantly distorted due to the SPD. Possibly, this was a consequence of great stresses appearing inside the grains and the accumulation of a great number of dislocations on the grains' boundaries. The diffraction halo (Figure 7b) revealed at the depth of 5 μm indicates the presence of a strongly fragmented NCS, which is nearly amorphous. Fuzzy diffraction rings (Figure 7d) at the depth of 10 μm point to the formation of an NCS, the presence of diffraction reflexes indicate the high disorientation of grain and reflex coalescences, and

these are reflected in the middle and low disorientations of the part of the grains. Such diffraction patterns are typical of NCSs.

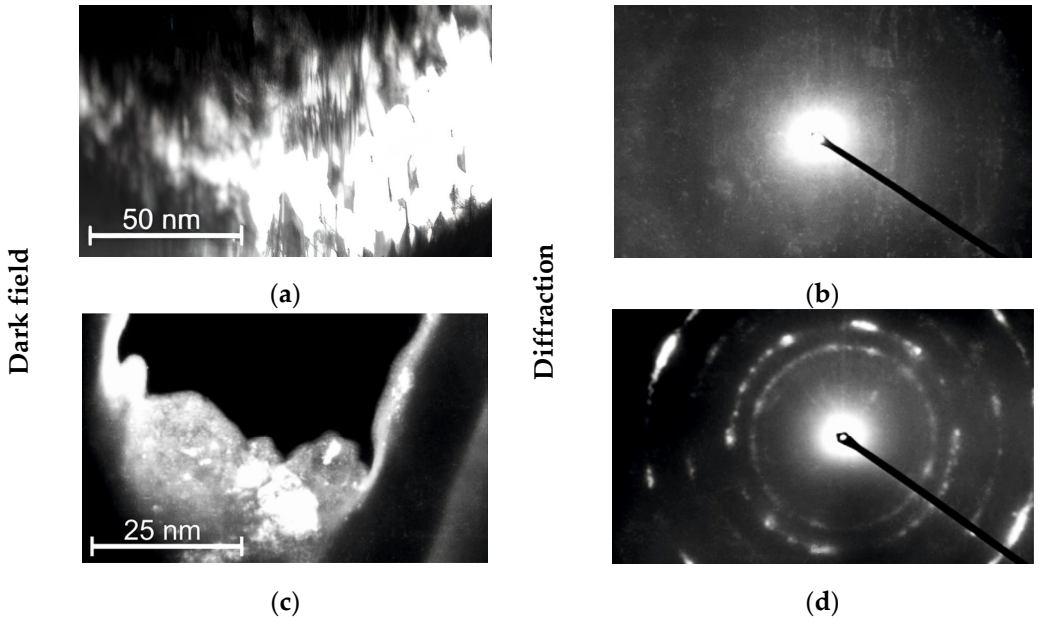

Figure 7. Electron microscope images (**a**,**c**) and diffraction patterns (**b**,**d**) of steel C45 after the MPT made at depths of 5 (**a**,**b**) and 10 μm (**c**,**d**).

The average weight losses of the investigated friction pair, Steel 41Cr4 and Cast iron GJL-200, during the wear tests have been presented in Figure 8a, and the average friction coefficients and temperature in the friction zone are shown in Figure 8b.

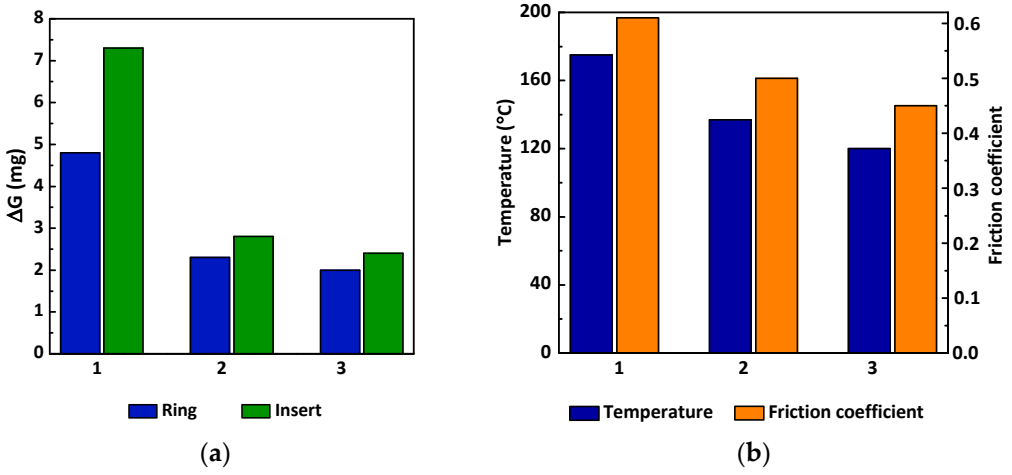

Figure 8. Wear resistance of the friction pair, Steel 41Cr4 and Cast-iron GJL-200, (the weight loss of specimen' friction pair (V = 0.9 m/s, P = 1 MPa, t = 6 h) (**a**); temperature and friction coefficient in the friction zone (**b**)): non-strengthened one (1) after the MPT using the tool with the smooth working surface (2) and with the oppositely directed grooves on the working surface (3).

Conducting the MPT using both of the tools significantly increased the wear resistance of the friction pairs. Thus, the wear resistance of the ring specimens made of steel 41Cr4 and strengthened using the tool with the oppositely directed grooves on the working surface was increased by 2.4 times compared to that of the non-strengthened pair. The ring specimen, the contact surfaces of which were strengthened using the tool with the smooth

working surface, was characterised by a slightly smaller increase in the wear resistance (by 2.1 times).

After analysing the wear resistance of the insert specimens made of grey cast iron, it should be emphasised that their contact surfaces were not subjected to the MPT. However, their wear resistance in the friction pair with the strengthened ring specimens was also increased. Thus, the weight losses of the insert specimens that worked in a pair with the ring specimens, which were strengthened by the MPTs using tools with smooth working surfaces and with the oppositely directed grooves on the working surface, were decreased by 2.6 and 3 times, respectively (Figure 8a). The friction coefficient of the pair and the temperature in the sliding zone also decreased (Figure 8b). The increase in the wear resistance of friction pairs after the MPT and the decrease in friction coefficients and temperature in the sliding zone can be explained by the formation of a strengthened surface layer with the NCS. Grinding the structure of the strengthened layer to the nanoscale, changing the phase and chemical composition [11], stress state, and increasing the microhardness, etc., contributed to the enhancement of the operational characteristics and, in this case, the wear resistance of the friction pairs [41,42]. High-quality, continuous secondary structures were formed on the contact surfaces of the strengthened layers with the NCS during friction, as demonstrated in [43], which lead to decreases in the temperature and in the coefficient of friction in the sliding zone and to an increase in the wear resistance of the friction pair as a whole.

The contact interaction of the parts' surfaces determines the actual contact area, contact stiffness, the magnitude of local stresses, the conditions for the formation of the oil film (in the presence of the oil lubrication), and other factors that affect the operational characteristics of the machine parts. Figure 9 shows a view of the surface topography of the specimens after the MPT using the tools with different working parts. The analysis of the topographies of the treated surfaces showed that they depend on the shape of the working surfaces of the tool. After the MPT, the roughness of the specimens with the smooth working surface was 0.49 μm, and that of the specimens after the MPT with the oppositely directed grooves on the working surface was 0.37 μm.

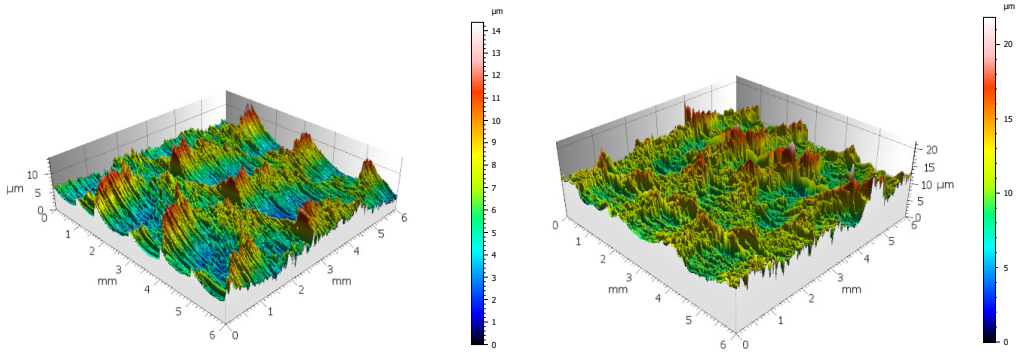

(**a**) (**b**)

Figure 9. Topography of the treated surface after the MPT using the tool with the smooth working surface (**a**) and with the oppositely directed grooves on the working surface (**b**).

The shear deformation of the treated surface metal occurred only in the direction of the rotation of the tool with the smooth working surface. The quality parameters of the treated surface formed due to the friction caused by the tool in one direction along the contact surface of the part. The waviness of the surface is different in the longitudinal and transverse directions, as shown in Figure 10. In the transverse direction (perpendicular to the direction of the treatment), the height of the peaks is approx. 7 μm, and it has a pitch of about 2 mm, which is equal to the magnitude of the cross feed of the tool. In the longitudinal direction, the waviness was not accurately measured. The height of the profile is also about 9 μm, and the pitch is indefinite (Figures 9 and 10).

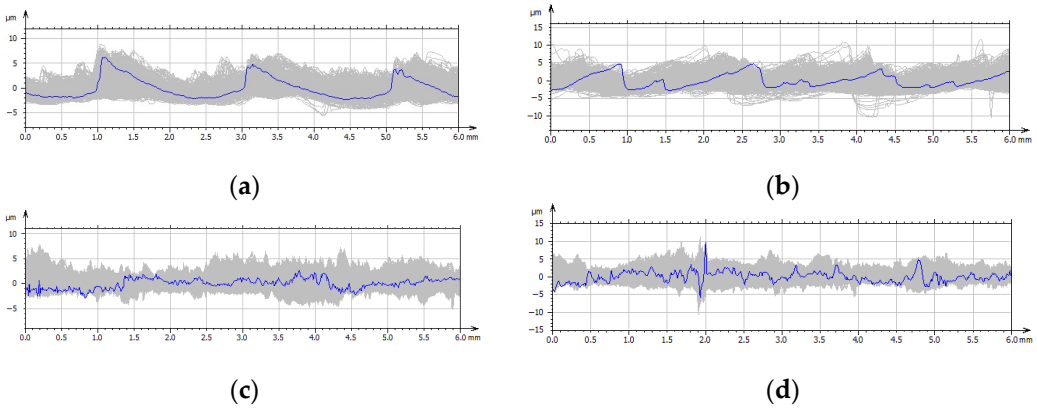

Figure 10. The waviness (**a**,**c**) and roughness (**b**,**d**) of the steel surface after the MPT using the tool with the smooth working surface (**a**,**b**) and the tool with the oppositely directed grooves on the working surface (**c**,**d**).

In the case of the MPT using the tool with the oppositely directed grooves on the working surface, the shear deformation of the metal on the treated surface layer occurs not only in the direction of the tool's rotation, but also in the direction perpendicular to the slope of the groove with an opposite sign. An additional oscillating deformation is due to the action of the oppositely directed grooves. The formation of the quality parameters of the treated surface is due to the friction of the smooth part of the tool and the opposite movement of the inclined groove on the contact surface of the workpiece. Based on the features of topography defined in [44], the results of the analysis of the topographies of the treated surfaces (see Figure 9) show that the location of the peaks is more uniform for the surface after the MPT with the tool with the oppositely directed grooves on the working surface than it is after the treatment using another tool. The surface waviness in the transverse direction is more pronounced than it is in the longitudinal one (Figure 10). In the transverse direction (perpendicular to the direction of treatment), the wave height is about 5 µm. In this case, the pitch is variable, and it is approx. 1.5 mm. It is smaller than the magnitude of the transverse feed applied in the MPT is. The pitch of waviness was not accurately measured in the longitudinal direction. The formation of the quality parameters of the treated surface during strengthening using the tool with the oppositely directed grooves on the working surface is due to the complex deformation of the contact zone of the tool and specimen. The metal in the contact area deforms in a direction that coincides with the direction of the tool rotation and in the perpendicular direction as well.

One of the important parameters of the quality of the treated surface, which is determined by the stereometric parameters, is its bearing capacity. The bearing area curve (Abbott–Firestone curve) characterises the behaviour of the surface under the friction process. It determines the real area of the surface, which is at different depths of the distorted (deformed) profile, and the volume that occupies the material of the metal and void. There are three characteristic areas on the surface-bearing capacity curve: the first one is the area of the peaks with a large height that wears during the running in of the connected surfaces of the friction pair, while the second one is the area of peaks with a medium height, which is the basis of the profile and determines the load-bearing capacity of the surface, affecting the durability of the test surface in the friction process and the amount of permissible wear of the pair as a whole, and the third one is the area of the depression, the depth of which characterises the ability to keep the lubricant on the surface. The evaluation of the running-in process and the wear of the contact surfaces of the friction pair can be performed using the Abbott–Firestone diagram. The representative Abbott–Firestone diagram for the friction pair is presented in Figure 11. The area and volume of the depression (lubricant 'pockets') where the lubricant resides is a very important factor in the friction process, and it is evaluated using the bearing curve.

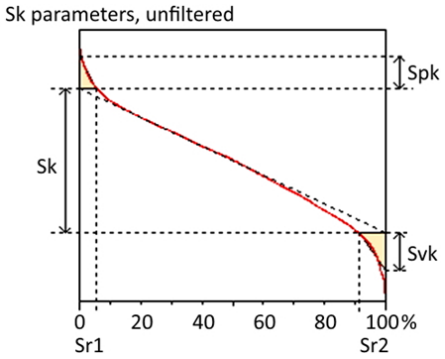

Figure 11. Abbott–Firestone diagram. S_k is core height, S_{pk} is reduced peak height, S_{vk} is reduced dale height, S_{r1} and S_{r2} is material ratios.

Table 2 presents the data on the bearing capacity of the friction pair, Steel 41Cr4 and Cast-iron GJL-200, after the MPT using the tools with different working parts and without the treatment. The functional parameters, namely the height of the peaks Spk on the bearing capacity curve, the magnitude of the slope of the curve Sk, and the depth of the depressions Svk, were determined from the Abbott–Firestone diagrams.

Table 2. Bearing capacity data of the friction pair, Steel 41Cr4 and Cast-iron GJL-200.

MPT	Sk, μm	Spk, μm	Svk, μm	Sr1, %	Sr2, %
Without	6.05	1.36	1.55	5.64	91.1
Tool with the smooth working surface	4.55	2.68	0.773	13.6	94.9
Tool with the oppositely directed grooves	3.19	1.64	1.07	12.6	91.8

The parameter of the bearing capacity curve Sk, which determines the slope of the curve, is the smallest one after the MPT using the tool with the oppositely directed grooves on the working surface among the studied friction pairs. This parameter determines the stabilised period of the friction pair. When the value of the slope is smaller, the durability of this surface is greater, which was confirmed experimentally by the wear tests. The slope of the curve at a smaller angle shows that the real surface of the contact surface is greater, respectively, which will resulted in a lower unit load in the friction zone. Under these conditions, the temperature of the contact surfaces of the friction pair decreased and the intensity of wear of the contact parts was reduced, which increased the durability of the friction pair.

The location of the peaks on the strengthened surface of the specimens after the MPT using the tool with the oppositely directed grooves on the working surface is uniform compared to that for the surface that was strengthening using the tool with the smooth working surface. The slope of the middle section of the bearing capacity curve (Abbott–Firestone diagram), which determines the durability of the friction pair, is the smallest one (Sk = 3.19 μm) after the MPT using the tool with the oppositely directed grooves on the working surface. After strengthening it using the tool with the smooth working surface, the slope is higher, and it is Sk = 4.55 μm. For the non-strengthened (which were ground after quench hardening and low-temperature tempering) specimens, the slope of the bearing capacity curve is the highest one, and it is Sk = 6.05 μm, which is consistent with the results of the wear resistance studies.

4. Conclusions

The influence of unidirectional and multidirectional SPDs on the formation and properties of the nanocrystalline surface layer on low alloy steel 41Cr4 were studied in this work.

The parameters of the surface NCS (grain size, phase composition, depth of the treated layer, microhardness, wear resistance, topography, and bearing capacity) depended on the deformation mode during the MPT.

The multidirectional SPD of the treated surface layer of specimens made of steel 41Cr4 by the MPT using the tool with the oppositely directed grooves on the working surface facilitates the generation of dislocations and the dispersion of the structure, which contribute to an increase in the depth, microhardness, and to a decrease in the grain size of the formed NCS compared to that of the unidirectional SPD (using the tool with the smooth working surface).

The wear resistance of the nanocrystalline surface of steel 41Cr4 in the friction pair with cast iron GJL-200 is considerably higher than that of the heat-treated one. The highest wear resistance of the nanocrystalline surface of steel 41Cr4 is observed after the MPT using the tool with the oppositely directed grooves on the working surface (it is 2.4 times higher compared to that of the non-strengthened pair). It was also associated with the formation of favourable surface topography and parameters of the bearing capacity curve.

The multidirectional SPD should be considered as a more effective mechanism for surface NCS formation compared with the unidirectional one (simple shear) because it produces an increase in the working capacity of the friction pairs due to the higher microhardness and thickness of the strengthened surface layer, as well as a more favourable surface topography.

Author Contributions: Conceptualization, V.K., I.H. and O.Z.; methodology, O.M., V.G. and Y.K.; formal analysis, V.K., I.H., O.M., V.G., Y.K. and O.Z.; investigation, V.K., I.H. and O.Z.; validation, O.M., V.G. and Y.K.; writing—original draft preparation, V.K., I.H., O.M., V.G., Y.K. and O.Z.; writing—review and editing, V.K. and I.H.; supervision, V.K. and I.H. All authors have read and agreed to the published version of the manuscript.

Funding: This research received no external funding.

Institutional Review Board Statement: Not applicable.

Informed Consent Statement: Not applicable.

Data Availability Statement: Not applicable.

Conflicts of Interest: The authors declare no conflict of interest.

References

1. Dwivedi, D.K. *Surface Engineering. Enhancing Life of Tribological Components*; Springer: New Delhi, India, 2018. [CrossRef]
2. Quintino, L. *Overview of coating technologies In: Surface Modification by Solid State Processing*; Miranda, R., Ed.; Elsevier: Cambridge, UK, 2014; pp. 1–24. [CrossRef]
3. Kaplun, P.V.; Honchar, V.A.; Donchenko, T.V. Wear kinetics of steels with diffusion coatings in rolling friction. *Mater. Sci.* **2020**, *56*, 50–58. [CrossRef]
4. Zhai, W.; Bai, L.; Zhou, R.; Fan, X.; Kang, G.; Liu, Y.; Zhou, K. Recent progress on wear-resistant materials: Designs, properties, and applications. *Adv. Sci.* **2021**, *8*, 2003739. [CrossRef] [PubMed]
5. Bhadauria, N.; Pandey, S.; Pandey, P.M. Wear and enhancement of wear resistance—A review. *Mater. Today Proc.* **2020**, *26*, 2986–2991. [CrossRef]
6. Kuang, W.; Miao, Q.; Ding, W.; Li, H. A short review on the influence of mechanical machining on tribological and wear behavior of components. *Int. J. Adv. Manuf. Technol.* **2022**, *120*, 1401–1413. [CrossRef]
7. Umemoto, M.; Todaka, K.; Tsuchiya, K. Formation of nanocrystalline structure in carbon steels by ball drop and particle impact techniques. *Mater. Sci. Eng. A* **2004**, *375–377*, 899–904. [CrossRef]
8. Dai, K.; Shaw, L. Comparison between shot peening and surface nanocrystallization and hardening processes. *Mater. Sci. Eng. A* **2007**, *463*, 46–53. [CrossRef]
9. Fu, Y.; Wang, G.; Gao, J.; Yao, Q.; Tong, W. New approach to produce a nanocrystalline layer on surface of a large size pure titanium plate. *Coatings* **2020**, *10*, 430. [CrossRef]
10. Olugbade, T.O.; Lu, J. Literature review on the mechanical properties of materials after surface mechanical attrition Treatment (SMAT). *Nano Mater. Sci.* **2020**, *2*, 3–31. [CrossRef]

11. Nykyforchyn, H.; Kyryliv, V.; Maksymiv, O.; Zvirko, O. Mechanical fabrication methods of nanostructured surfaces. In *Handbook of Modern Coating Technologies. Fabrication Methods and Functional Properties*; Aliofkhazraei, M., Ali, N., Chipara, M., Laidani, N.B., De Hosson, J.T.M., Eds.; Elsevier: Amsterdam, The Netherlands, 2021; pp. 25–67. [CrossRef]
12. Estrin, Y.; Vinogradov, A. Extreme grain refinement by severe plastic deformation: A wealth of challenging science. *Acta Mater.* **2013**, *51*, 782–817. [CrossRef]
13. Nykyforchyn, H.; Kyryliv, V.; Maksymiv, O. Physical and mechanical properties of surface nanocrystalline structures, generated by severe thermal-plastic deformation. In *Nanocomposites, Nanophotonics, Nanobiotechnology, and Applications*; Fesenko, O., Yatsenko, L., Eds.; Springer: Cham, Switzerland, 2014; pp. 31–41. [CrossRef]
14. Zhang, W.; Chen, X.; Yang, C.; Wang, X.; Zhang, Y.; Li, Y.; Huan, X.; Zhong, Z. A multiphysics model for predicting microstructure changes and microhardness of machined AerMet100 steel. *Materials* **2022**, *15*, 4395. [CrossRef]
15. Grosdidier, T.; Novelli, M. Recent developments in the application of surface mechanical attrition treatments for improved gradient structures: Processing parameters and surface reactivity. *Mater. Trans.* **2019**, *60*, 1344–1355. [CrossRef]
16. Tao, N.; Lu, J.; Lu, K. Surface nanocrystallization by surface mechanical attrition treatment. *Mater. Sci. Forum* **2004**, *579*, 91–108. [CrossRef]
17. Edalati, K.; Bachmaier, A.; Beloshenko, V.; Beygelzimer, Y.; Blank, V.; Botta, W.; Bryla, K.; Cizek, J.; Divinski, S.; Enikeev, N.; et al. Nanomaterials by severe plastic deformation: Review of historical developments and recent advances. *Mater. Res. Lett.* **2022**, *10*, 163–256. [CrossRef]
18. Guan, X.S.; Dong, Z.F.; Li, D.Y. Surface nanocrystallization by sandblasting and annealing for improved mechanical and tribological properties. *Nanotechnology* **2005**, *16*, 2963–2971. [CrossRef]
19. Wang, X.Y.; Li, D.Y. Mechanical, electrochemical and tribological properties of nano-crystalline surface of 304 stainless steel. *Wear* **2003**, *255*, 836–845. [CrossRef]
20. Lesyk, D.A.; Maartinez, S.; Mordyuk, B.N.; Dzemelinskyi, V.V.; Lamikiz, A.; Prokopenki, G.I. Effects of laser heat treatment combined with ultrasonic impact treatment on the surface topography and hardness of carbon steel AISI 1045. *Opt. Laser Technol.* **2019**, *111*, 424–438. [CrossRef]
21. Majerlik, J.; Barenyi, I.; Eckert, M. Investigation of mechanical properties of hard finish turned and grinded surfaces. *Procedia Struct. Integr.* **2019**, *23*, 541–546. [CrossRef]
22. Peral, L.B.; Quintero, A.; Vielma, A.T.; Barbes, M.F.; Fernandez-Pariantr, I. TEM evaluation of steel nanocrystalline surfaces obtained by severe shot peening. *Surf. Coat. Tech.* **2021**, *418*, 127238. [CrossRef]
23. Tao, N.R.; Wang, Z.B.; Tong, W.P.; Sui, M.L.; Lu, J.; Lu, K. An investigation of surface nanocrystallization mechanism in Fe induced by surface mechanical attrition treatment. *Acta Mater.* **2002**, *50*, 4603–4616. [CrossRef]
24. Kokkirala, S.; Holmberg, J.; Klement, U.; Lundstrom, R.; Iwasaki, H.; Hosseini, S.B. Effect of cutting parameters on the generated surface integrity of hard-turned martensitic AISI 52100 bearing steel. *Proc. CIPR* **2022**, *115*, 154–159. [CrossRef]
25. Li, J.G.; Umemoto, M.; Tokada, Y.; Tsuchiya, K. Role of strain gradient on the formation of nanocrystalline structure produced by severe plastic deformation. *J. Alloys Compd.* **2007**, *434–435*, 290–293. [CrossRef]
26. Li, Y.; Raabe, D.; Herbig, M.; Choi, P.P.; Goto, S.; Kostka, A.; Yarita, H.; Borchers, C.; Kirchheim, R. Segregation stabilizes nanocrystalline bulk steel with near theoretical strength. *Phys. Rev. Lett.* **2014**, *113*, 106104. [CrossRef]
27. Hull, D.; Bajcon, D.J. Origin and multiplication of dislocations. In *Introduction to Dislocations*, 5th ed.; Butterworth-Heinemann: Oxford, UK, 2011; pp. 157–169. [CrossRef]
28. Van Swygenhoven, H.; Derlet, P.M.; Froseth, A.G. Nucleation and propagation of dislocations in nanocrystalline fcc metals. *Acta Mater.* **2006**, *54*, 1975–1983. [CrossRef]
29. Estrin, Y.; Kim, H.S.; Nabarro, F.R.N. A comment on the role of Frank–Read sources in plasticity of nanomaterials. *Acta Mater.* **2007**, *55*, 6401–6407. [CrossRef]
30. Li, J.C.M.; Feng, C.R.; Rath, B.B. Emission of dislocations from grain boundaries and its role in nanomaterials. *Crystals* **2021**, *11*, 41. [CrossRef]
31. Kyryliv, V.I.; Gurey, V.I.; Maksymiv, O.V.; Hurey, I.V.; Kulyk, Y.O. Influence of the deformation mode on the force conditions of formation of the surface nanostructure of 40KH steel. *Mater. Sci.* **2021**, *57*, 422–427. [CrossRef]
32. Tondro, A.; Taharijam, M.; Abdolvand, H. Diffusion and redistribution of hydrogen atoms in the vicinity of localized deformation zones. *Mech. Mater.* **2022**, *177*, 104544. [CrossRef]
33. Nykyforchyn, H.M.; Lunarska, E.; Kyryliv, V.I.; Maksymiv, O.V. Hydrogen permeability of the surface nanocrystalline structures of carbon steel. *Mater. Sci.* **2014**, *50*, 67–73. [CrossRef]
34. Hurey, I.; Hurey, T.; Gurey, V. Wear resistance of hardened nanocrystalline structures in the course of friction of steel-grey cast iron pair in oil-abrasive medium. In *Advances in Design, Simulation and Manufacturing II. DSMIE 2019*; Lecture Notes in Mechanical, Engineering; Ivanov, V., Trojanowska, J., Machado, J., Liaposhchenko, O., Zajac, J., Pavlenko, I., Edl, M., Perakovic, D., Eds.; Springer: Cham, Switzerland, 2020; pp. 572–580. [CrossRef]
35. Gurey, V.; Hurey, I.; Hurey, T.; Wojtowicz, W. Fatigue strength of steel samples after friction treatment. In *Advanced Manufacturing Processes IV. InterPartner 2022.Lecture Notes in Mechanical Engineering*; Tonkonogyi, V., Ivanov, V., Trojanowska, J., Oborskyi, G., Pavlenko, I., Eds.; Springer: Cham, Switzerland, 2023; pp. 274–283. [CrossRef]
36. Kyryliv, V.; Chaikovs'kyi, B.; Maksymiv, O.; Mykytchak, B. Fatigue and corrosion fatigue of the roll steels with surface nanostructure. *J. Nano Res.* **2018**, *51*, 92–97. [CrossRef]

37. Gurey, V.; Shynkarenko, H.; Kuzio, I. Mathematical model of the thermoelasticity of the surface layer of parts during discontinuous friction treatment. In *Advanced in Design, Simulation and Manufacturing IV. DSMIE 2021*; Ivanov, V., Pavlenko, I., Liaposhchenko, O., Machado, J., Edl, M., Eds.; Lecture Notes in Mechanical Engineerin; Springer: Cham, Switzerland, 2021; pp. 12–22. [CrossRef]
38. Krous, W.; Nolze, G. Powder Cell—A program for the representation and manipulation of crystal structures and calculation of the resulting X-ray powder patterns. *J. Appl. Cryst.* **1996**, *29*, 301–303. [CrossRef]
39. *Powder Diffraction File Search Manual [inorganic]: Alphabetical Listing and Search Section of Frequently Encountered Phases*; Joint Committee on Powder Diffraction Standards: Philadelphia, PA, USA, 1976.
40. *ISO 25178–26:2012*; Geometrical Product Specifications (GPS)—Surface Texture: Profile Method—Part 2: Terms, Definitions and Surface Texture Parameters (IDT); ISO 26178–26. International Organization of Standardization: Geneva, Switzerland, 2012.
41. Li, G.; Guan, D. Friction and wear behaviors of nanocrystalline surface layer of medium carbon steel. *Tribol. Int.* **2010**, *43*, 2216–2221. [CrossRef]
42. Kyryliv, Y.; Kyryliv, V.; Tsizh, B.; Maksymiv, O. Resistance of surface nanostructures and ultrafine grain structures on steel 40Kh to wear and cavitation-erosive destruction. *Appl. Nanosci.* **2022**, *12*, 1085–1090. [CrossRef]
43. Hutchings, I.; Shipway, P. *Tribology. Friction and Wear of Engineering Materials*, 2nd ed.; Butterworth-Heinemann: Oxford, UK, 2017.
44. Jiang, X.; Senin, N.; Scott, P.J.; Blateyron, F. Feature-based characterisation of surface topography and its application. *CIRP Ann.* **2021**, *70*, 681–702. [CrossRef]